



# Geochemistry and geochronology of pre-Brasiliano rocks from the Transversal Zone, Borborema Province, Northeast Brazil

J.M. Sá<sup>a,\*</sup>, J.M. Bertrand<sup>b</sup>, J. Leterrier<sup>c</sup>, M.H.F. Macedo<sup>a</sup>

<sup>a</sup>*Departamento de Geologia, Universidade Federal do Rio Grande do Norte, Campus Universitário, 59078-970 Natal, RN, Brazil*

<sup>b</sup>*LGCA Campus Scientifique, F 73376 Le Bourget du Lac, France*

<sup>c</sup>*CRPG/CNRS, 15 Rue Notre Dame des Pauvres, 54501 Vandoeuvre, France*

Received 1 March 2001; accepted 1 August 2001

## Abstract

Proterozoic metamorphosed sequences are identified in the Transversal Zone (TZ) domain of the Borborema geological province, Northeast Brazil. This TZ domain is located between the well-known E–W Patos and Pernambuco continental shear zones. In its eastern part, in the Taquaritinga region, a large mass of augen gneisses with a conspicuous horizontal to subhorizontal tectonic foliation forms one of the most important rock types in the region that displays U–Pb zircon ages ca. 1.52 Ga. Paleoproterozoic orthogneisses dated by U–Pb on zircon at ca. 1.97 Ga and older paragneisses and banded gneisses represent basement rocks, which were cross-cut by these Mesoproterozoic augen gneisses, and have been in turn intruded by plutonic rocks in upper Neoproterozoic (U–Pb and Rb–Sr, ca. 0.6 Ga) times.

Chemical analyses of major, minor, and trace elements (including REE) for the basement orthogneisses indicate calcalkaline affinities and a signature very similar to volcanic arc granites, representing crustal accretion during the Paleoproterozoic Transamazonian/Eburnean orogenesis in the region. In turn, the chemical data for augen gneisses indicate that they are relatively homogeneous and evolved metaluminous metaplutonic rocks with characteristics very similar to A-type granites generated and emplaced in an extensional anorogenic setting. Relatively high  $^{87}\text{Sr}/^{86}\text{Sr}$  initial ratio and negative  $\varepsilon_{\text{Nd}(t)}$  are signatures of crustal components in these rocks.

Based on geochemical, geochronological, and structural data, the Taquaritinga region is composed of Paleoproterozoic (>1.97 Ga) rocks intruded by Mesoproterozoic (ca. 1.5 Ga) anorogenic granites and Neoproterozoic granites (ca. 0.6 Ga). These data also suggest that the tectonometamorphic structures displayed by Meso and Neoproterozoic suites were developed by the Brasiliano/Pan-African orogeny and that the record of Transamazonian/Eburnean orogeny is restricted to basement rocks. This means that there is no evidence for a compressional event in Mesoproterozoic times (Cariris Velhos = Grenville) as suggested for the central and western part of the TZ. It is important to remark that the Taquaritinga augen gneisses are, up to now, the only unit that represents magmatic pulses associated with extensional episodes with this age (ca. 1.5 Ga) in the TZ and in the whole Borborema Province. © 2002 Elsevier Science Ltd. All rights reserved.

## Resumo

A zona Transversal da Província Borborema está geologicamente situada entre os lineamentos Pernambuco e Patos. Na sua parte oriental, na região de Taquaritinga (PE), dominam augen gnaisses com uma penetrativa e proeminente foliação tectônica subhorizontal, com idade de cristalização de 1.52 Ga obtida em zircão. Estas rochas são intrusivas em ortognaisses e paragnaisses do embasamento com idade mínima em torno de 1.97 Ga, e são intrudidas por rochas plutônicas associadas ao Ciclo Brasileiro (ca. 0.6 Ga).

Análises de elementos maiores, menores e traços (incluindo terras raras) nos augen gnaisses mostram caráter metaluminoso para esta suíte ígnea e fortes semelhanças com os granitos tipo-A gerados em ambiente anorogênico. Razões iniciais  $^{87}\text{Sr}/^{86}\text{Sr}$  relativamente altas e  $\varepsilon_{\text{Nd}(t)}$  negativos são assinaturas indicadoras de forte contribuição crustal nestes augen gnaisses.

A conjunção dos dados geoquímicos, geocronológicos e de campo indicam que na região de Taquaritinga onde são identificadas rochas de idades paleo (>1.95 Ga), meso (ca. 1.5 Ga) e neoproterozóicas (ca. 0.6 Ga), o ciclo orogênico Transamazônico é restrito às rochas do embasamento, e que todas as estruturas dúcteis identificadas nas rochas meso e neoproterozóicas foram desenvolvidas durante o Ciclo orogênico Brasileiro. Não foram encontradas evidências que atestem a existência do Ciclo Cariris Velhos nesta parte da Província Borborema. Contudo, está bem marcado que nesta Zona Transversal e na Província Borborema, os augen gnaisses de Taquaritinga são, até o momento, os únicos marcadores de pulsos magmáticos associados com eventos extensionais crustais datados do Mesoproterozóico inferior. © 2002 Elsevier Science Ltd. All rights reserved.

\* Corresponding author. Tel.: +55-842-153-780; fax: +55-842-153-640.

E-mail address: jaziel@geologia.ufrn.br (J.M. Sá), jean-michel.bertrand@univ-savoire.fr (J.M. Bertrand), jblet@club-internet.fr (J. Leterrier).

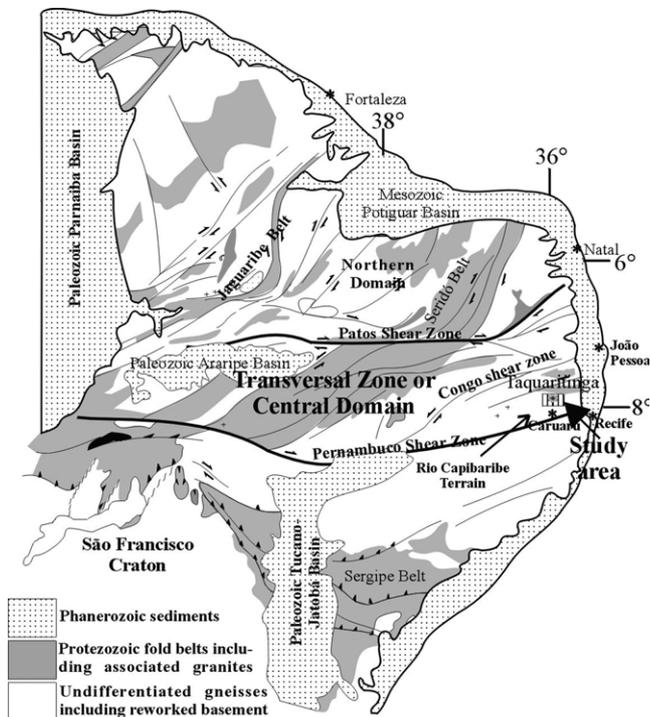


Fig. 1. Location of the Taquaritinga region and main domains of the Borborema geological Province, northeastern Brazil.

## 1. Introduction

In Northeast Brazil the Borborema Province is the name of the assemblage of several Brasiliano/Pan-African fold belts (Almeida et al., 1977) comprising Archean/Paleoproterozoic basement. The province comprises an area of 500 000 km<sup>2</sup> and is located between the São Luiz/West African and São Francisco/Congo cratons occurring, respectively, to the north and to the south (Fig. 1).

This geological province is divided in three major domains delimited by the transcontinental E–W Patos and Pernambuco shear zones (Fig. 1). These strike-slip shear zones, together with the emplacement of voluminous granitoid plutons and batholiths, were formed in late Neoproterozoic times, during the Brasiliano/Pan-African orogenic cycle (ca. 0.6 Ga), which is the most important orogenic event responsible for the actual framework of the province.

The area discussed in this paper is located in the eastern part of the Transversal Zone (TZ), a domain situated between the two major shear zones. During the last decades, many arguments have been raised especially regarding the northern and central part of the Borborema Province, about the age of the older subhorizontal tectonic foliation, commonly displayed by augen gneisses and supracrustal rocks. Jardim de Sá and Hackspacher (1980), Jardim de Sá (1984), Macedo et al. (1984), and Bertrand and Jardim de Sá (1990) considered some of these structures and associated orthogneisses as late Paleoproterozoic in age

(Orosirian period) and corresponding to the Transamazonian/Eburnean orogenic cycle. In contrast, Caby (1989), Caby and Arthaud (1986), and Archanjo and Bouchez (1991) emphasized that the Brasiliano cycle is the only event responsible for all the ductile structures present in these belts, including those of the associated orthogneisses.

More recently and focusing on the TZ, a comprehensive review with a broad reevaluation of previous and new U–Pb and Sm–Nd data was carried out by Brito Neves et al. (1995a,b) and complemented by Van Schmus et al. (1995a,b), Kozuch et al. (1997), and Santos and Medeiros (1997), among others, who suggested a polycyclic evolution for the fold belts of this region. This evolution starts with a Mesoproterozoic crust-forming event comprising a collisional event (first compressional event) at ca. 1.0 Ga, the so-called Cariris Velhos (= Grenville) orogeny, followed by reworking during the Brasiliano Cycle (the second compressional event) at ca. 0.6 Ga. Archean to Paleoproterozoic banded gneisses, granodioritic to tonalitic orthogneisses and paragneisses that commonly display migmatitic textures and are cut by augen gneisses or are covered by volcanosedimentary sequences are defined as the basement units of the TZ and the effects of the Transamazonian/Eburnean orogeny (ca. 1.95 Ga) are, according to these authors, restricted to these basement rocks.

The Taquaritinga area is ideal to understand the pre-Brasiliano/Pan-African evolution of the TZ because it displays igneous plutonic rocks that intrude Paleoproterozoic rocks of the basement, which in turn are cut by well-dated Brasiliano/upper Neoproterozoic granitoid rocks. Taquaritinga is located in the eastern part of the Pajeú–Paraíba fold belt (Brito Neves, 1983), in the southeastern part of the TZ. Augen gneisses with a conspicuous subhorizontal foliation form one of the most important rock types present in the area. Would these augen gneisses have similar geochemical affinities and geodynamic evolution as other subalkaline to calcalkaline augen gneisses that occur in the TZ (central and western part) and to the north of the Patos shear zone? Is the flat foliation a Transamazonian (Paleoproterozoic) imprint, or is it a Cariris Velhos (late Mesoproterozoic) or even an early Brasiliano (late Neoproterozoic) tectonic fabric?

In addition to field relationships including the systematic use of structural criteria, and the geochronological dating—U–Pb, Sm–Nd, and Rb–Sr isotopic systematics on augen gneisses and basement orthogneisses—this paper documents the results of whole-rock chemical analyses, which provide information on the geotectonic evolution of the TZ, and discusses their implications to the previous knowledge of other regions of the Borborema Province.

## 2. Geological framework

Previous workers in the eastern part of the TZ, such as McMurry et al. (1987), Neves (1996), and Guimarães and

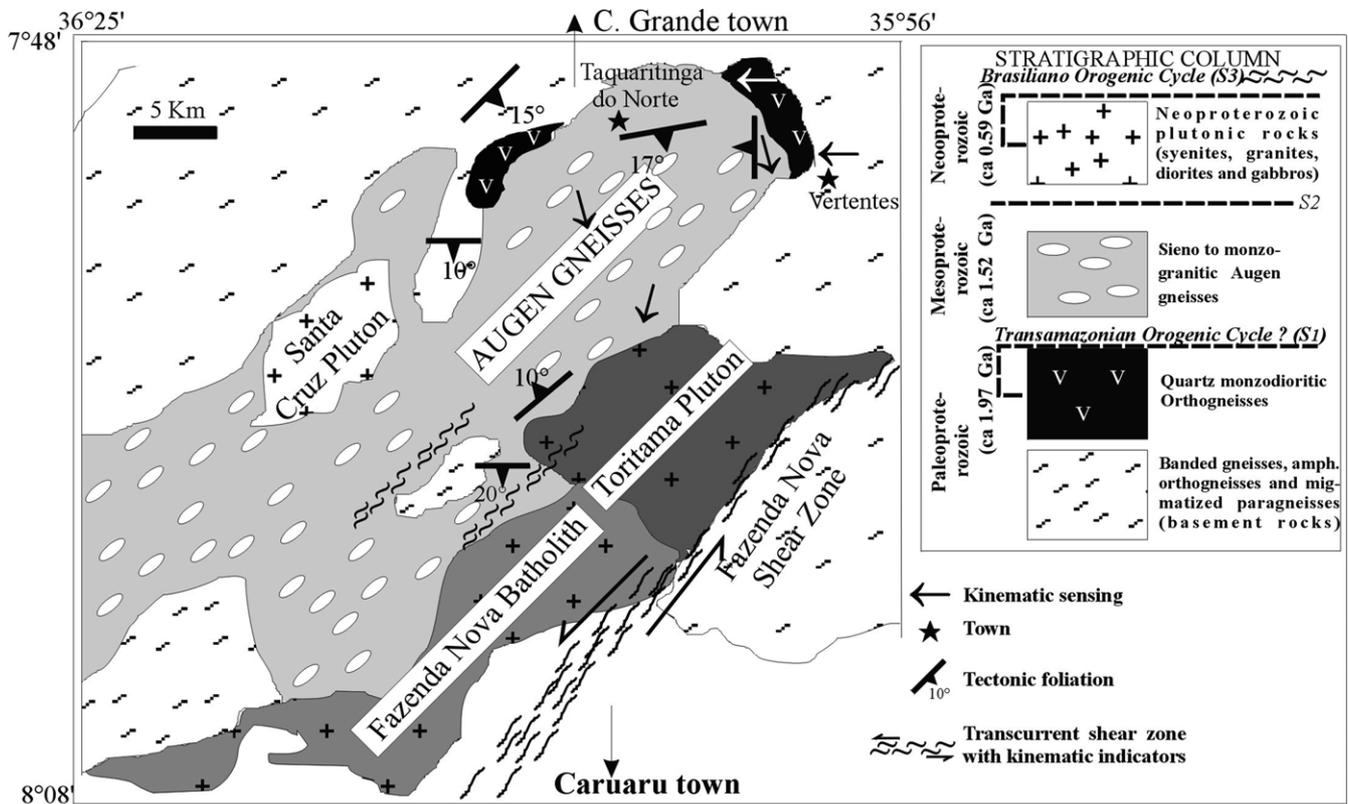


Fig. 2. Schematic geological map and stratigraphic column of the Taquaritinga region, northeast Brazil. Modified from Neves (1996).

Silva Filho (1997), have mainly emphasized the geochemistry and geodynamic evolution of the late Neoproterozoic granitoid plutons and batholiths, which are dominantly represented by syenites, monzonites, diorites, and gabbros.

U–Pb on zircon and whole-rock Rb–Sr data yielded  $592 \pm 7$  Ma and  $585 \pm 38$  Ma, respectively, for granites of the Toritama pluton (Guimarães and Silva Filho, 1997), in addition to the Rb–Sr age of  $630 \pm 34$  Ma obtained by McMurry et al. (1987) on granites from the neighboring Fazenda Nova batholith, characterizing these intrusions as late Neoproterozoic in age. Ar–Ar dating on amphibole and biotite (Neves, 1996) yielded ages of ca. 585 and 555 Ma for orthogneisses and granites, respectively. Many other mineral and whole-rock K–Ar results throughout the TZ and in the Borborema Province (i.e. Sá et al., 1995; Galindo et al., 1995; Souza, 1996) always reveal ages younger than 550 Ma, interpreted as cooling ages and/or marking the last tectonic event that has resetted the K–Ar or Ar–Ar isotopic system. Based on this statement, the Ar–Ar mineral dating of plutonic rocks of Taquaritinga indicates that closure/exhumation of the Brasiliano Cycle in this region took place at about 550 Ma ago.

The Brasiliano Toritama and Santa Cruz plutons and Fazenda Nova batholith are intrusive into basement orthogneisses, paragneisses, and migmatites, as well as in the augen gneisses that composes the Taquaritinga ridge.

Augen gneiss is the dominant lithology forming the ridge, which crops out for about  $400 \text{ km}^2$ , and reaches a topographic elevation of 1000 m above sea level in a region with average elevation of 450 m.

### 3. Structural relationships

Basement-banded gneisses, amphibole + garnet orthogneisses, micaschists and sillimanite + cordierite paragneisses form the northern and eastern rocks surrounding the Taquaritinga augen gneisses. The Toritama and Santa Cruz plutons and the Fazenda Nova batholith cross-cut them to the south and to the west (Fig. 2). The banded gneisses are characterized by interlayered centimetric to decimetric tonalitic and granitic bands, suggesting a predominant igneous protolith for these rocks (Fig. 3(a)).

Small bodies and sheets of quartz monzodioritic orthogneisses are also present. This rock type is particularly interesting because it cuts banded gneisses and paragneisses, but exhibits the same tectonic fabric and is intruded by the Taquaritinga augen gneisses, as displayed in the schematic stratigraphic cartoon of Fig. 4. This observation points out that the crystallization age of the quartz monzodioritic orthogneiss indicates a minimum age for the basement.

In the banded gneisses or orthogneisses and mainly in the

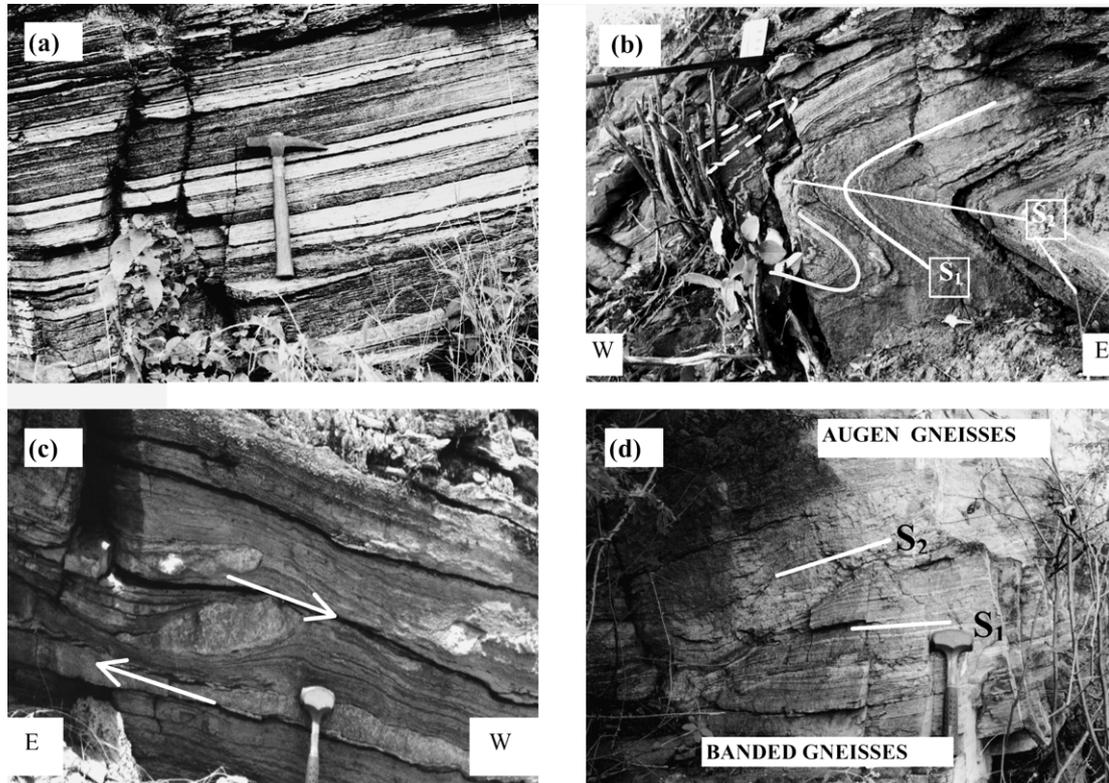


Fig. 3. (a) Homogeneous tonalitic (darker) and granitic compositional bands suggesting a predominant igneous protholite for the basement banded gneisses; (b) horizontal axial plane displayed by  $F_2$  tight folds which folds an earlier  $S_1$  metamorphic banding in paragneisses located close to Vertentes.  $L_x^1$  is E–W (parallel to the knife, in the upper left corner) in high angle to the direction of the  $F_2$  axis fold; (c) asymmetric boudins of granitic orthogneiss in basement paragneisses indicating a top to west kinematic sense. Outcrop located 1 km NE from Vertentes, on the main road; (d) augen gneiss cutting across the horizontal  $S_1$  banding of the basement banded gneiss and displaying a younger  $S_2$  subhorizontal tectonic fabric. Outcrop located 2.5 km west of Taquaritinga.

paragneisses, two subhorizontal and subparallel tectonic ( $S_1$  and  $S_2$  foliations) fabrics are always identified. The  $S_2$  foliation is related to tight (Fig. 3(b)) to isoclinal or transposed folds, sometimes turning parallel the  $S_1$  to  $S_2$  foliation in the limbs of isoclinal  $F_2$  folds. Type 3 (Ramsay, 1967)  $F_2/F_1$  interference patterns were observed mainly in micaschists and paragneisses. In addition, an E–W stretching lineation ( $L_x^1$ ) marked by quartz, feldspars, and sillimanite and a top-to-west kinematics marked by its asymmetry, are structural signatures observed in paragneisses and in the quartz monzodioritic orthogneisses. The same movement direction was also deduced from S–C structures and asymmetric boudins (Fig. 3(c)) observed on XZ outcrop sections. An important observation is that the E–W linear fabric ( $L_x^1$ ) has never been observed in the augen gneisses, suggesting that this stretching lineation direction is a tectonic marker imprinted in the basement rocks before the augen gneiss emplacement;  $L_x^1$  and  $S_1$  are hence restricted to the basement rocks, characterizing a tectonic discordance between the basement and the Taquaritinga augen gneiss body (Figs. 2 and 4). It is remarked that in the whole augen gneisses, a horizontal to subhorizontal tectonic foliation ( $S_2$ ) is ubiquitous, sometimes developing a metamorphic banding and/or subhorizontal mylonitic fabric.

The contact relationships between banded gneisses and the Taquaritinga augen gneisses are usually of tectonic origin and show a low-angle  $S_2$  mylonitic fabric. Furthermore, in some outcrops like the one situated 2.5 km along the main road, west from Taquaritinga, the augen gneiss cross-cuts the  $S_1$  metamorphic banding of the banded gneiss (Fig. 3(d)), and the  $S_2$  foliation is the first tectonic fabric present in the augen gneisses.

Elongated microcline megacrysts ( $L_x^2$ ) are a characteristic feature of the augen gneisses. They are sometimes divided in subgrains and/or recrystallized crystals up to 4 cm long on XZ and YZ planes. The absence or scarcity of stretching lineation and mylonitic fabric within this unit suggests a pure shear setting, despite some observed N160° stretching lineations ( $L_x^2$ ). Migmatization features associated with the subhorizontal  $S_2$  fabric have been observed near Taquaritinga, including neof ormation/recrystallization of microcline + garnet from destabilization of amphibole + biotite + plagioclase, developing bands richer in amphibole + biotite alternating with garnet + microcline.

The basement units and the augen gneisses and their subhorizontal tectonic fabrics are cross-cut by a younger steep dipping NE–SW striking tectonic fabric ( $S_3$ ), locally associated with stretching lineation related to the transcurrent Fazenda Nova shear zone. This  $S_3$  tectonic fabric

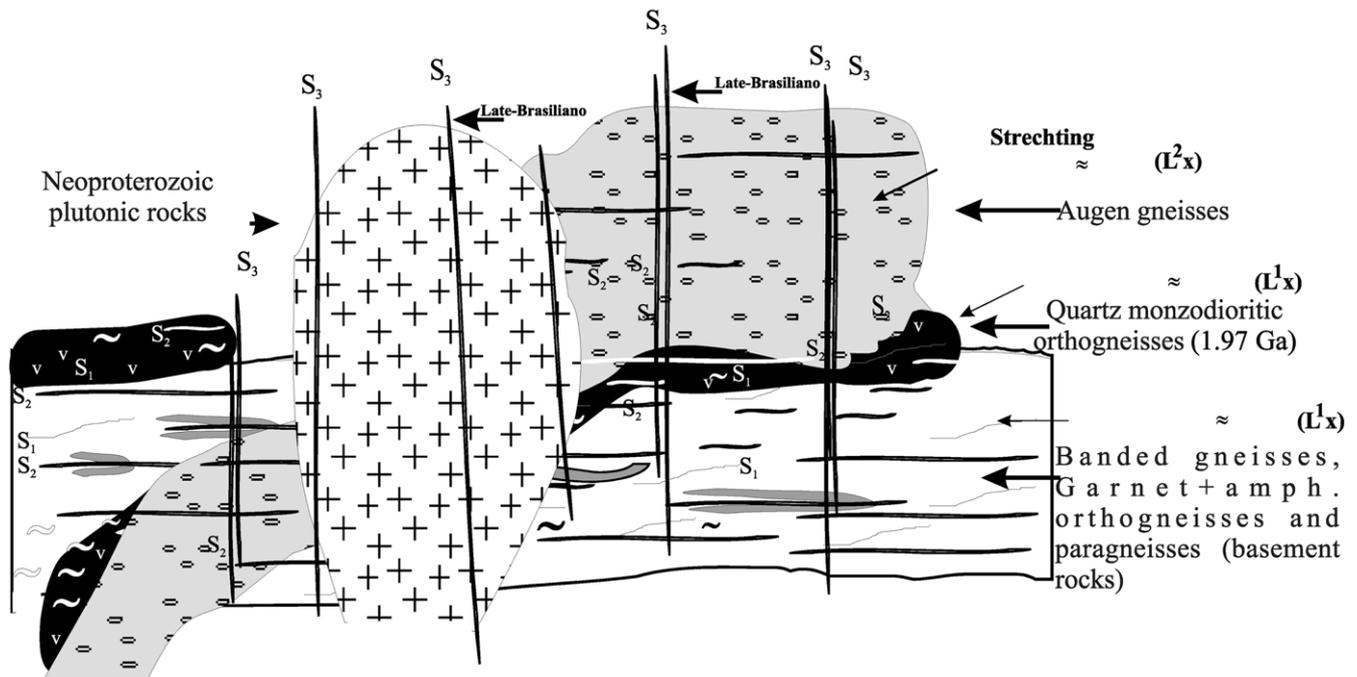


Fig. 4. Schematic stratigraphic column from Taquaritinga region, where  $S_1$  tectonic fabric is displayed only in banded gneisses, paragneisses and quartz monzodioritic orthogneisses. Note that the  $S_2$  foliation is the first tectonic fabric recorded by the augen gneisses.

is the only one displayed in the Neoproterozoic/Brasiliano granitoids (Fig. 4). The late Neoproterozoic rocks of the Fazenda Nova and Toritama bodies postdate the  $S_2$  foliation exhibited by the augen gneisses. Neves and Vauchez (1995) and Neves (1996) established a relative chronology for these late Neoproterozoic bodies considered as Brasiliano intrusions. In addition, Neves and Vauchez (1995) pointed out that the steeply dipping Fazenda Nova transcurrent shear zone ( $F_3$ ) was initiated during the last stages of crystallization of the Neoproterozoic intrusives but was still active after solidification of these bodies, developing a vertical to subvertical mylonitic foliation and a subhorizontal stretching lineation ( $L_3^3$ ) by the end of Neoproterozoic times.

#### 4. Geochronological data

Isotopic analyses were performed on augen gneisses to determine their crystallization age. The quartz monzodioritic orthogneisses were also dated to obtain the minimum age for the basement since they intrude the banded gneisses but are also affected by the  $F_1/D_1$  tectonic event, which is not the case of the Taquaritinga augen gneisses, only affected by  $F_2/D_2$ . For these analyses, samples have been chosen with no sign of alteration. Eventual fractures/joints have been cleaned up to avoid contamination or apport of elements outside the rock system.

U–Pb isotopic analyses were performed on non-magnetic zircon crystals. Several fractions were separated using criteria such as size, color, and shape. Before final hand-

picking and abrasion, the fractions were studied in Scanner Electronic Microscope (SEM) in order to identify possible inherited cores, internal structures, overgrowth, and/or metamorphic rims and types of inclusions. Some examples are shown in Fig. 5. Imaged zircon grains of Fig. 5 were separated of each fraction just before the final picking, so they do not represent exactly the analyzed grains because they were chosen to show the more complicated cases while the grains selected for analyses were the best quality zircon grains with no visible inclusions. Abrasion was done using pressure air with pyrite for 15–30 min. Picking, abrasion, zircon dissolution, as well as U and Pb chemical separation and mass spectrometric analysis were done in the Centre de Recherches Petrographiques et Geochimiques (CRPG/CNRS), at Nancy, France. A mixed  $^{235}\text{U}/^{208}\text{Pb}$  spike was used and common lead blanks determined for each batch of seven fractions, varied between 88 and 123 pg. Errors are given at the 95% confidence level and take into account the uncertainty on the measured ratios, common lead and the mass discrimination estimated from the repeated analyses of a standard (NBS 983) for each batch of seven fractions. Regression lines and ages have been calculated using Isoplot (Ludwig, 1999). More details of the procedure may be found in Bertrand et al. (1998).

Rb–Sr and Sm–Nd analyses were carried out at the geochemistry laboratory of the Geology Department of Rio Grande do Norte Federal University, at Natal, Brazil. Analytical procedures are described by Kawashita et al. (1974) for Rb and Sr and by Sato et al. (1995) for Sm and Nd separations. Isotopic Rb–Sr and Sm–Nd ratios were

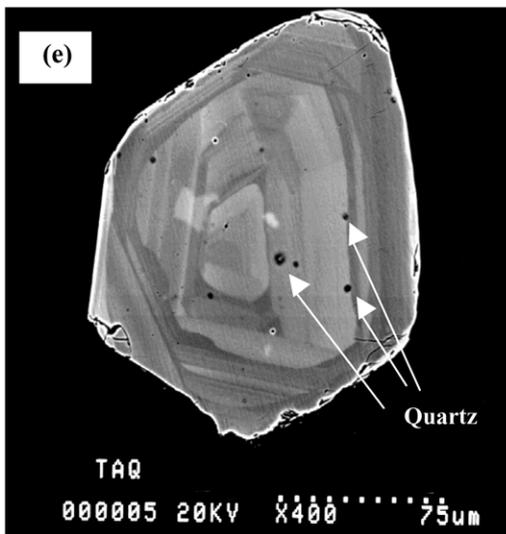
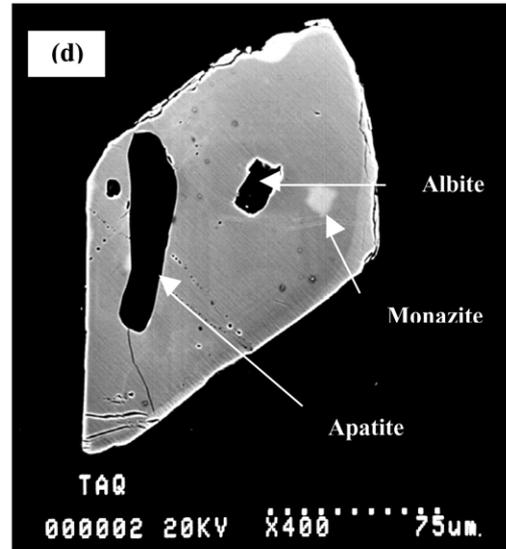
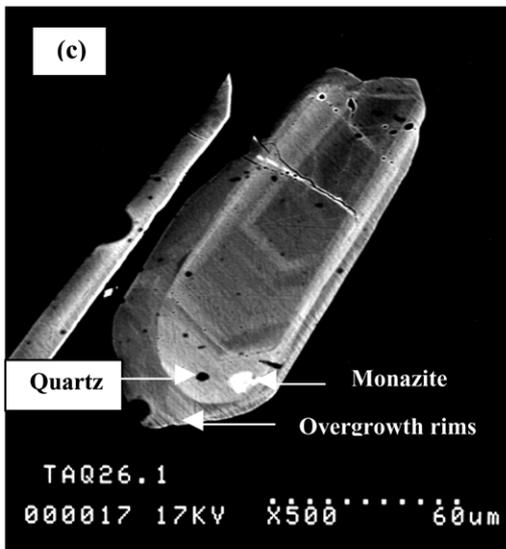
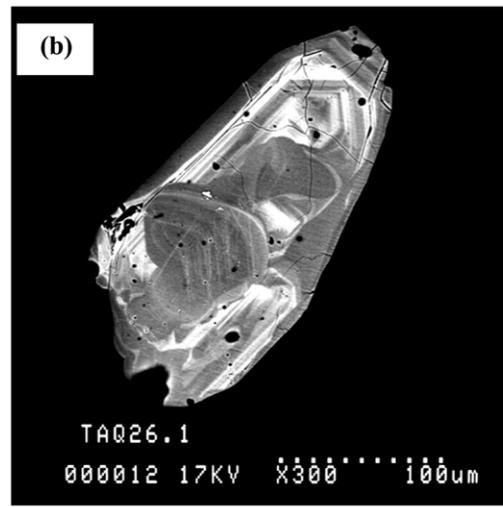
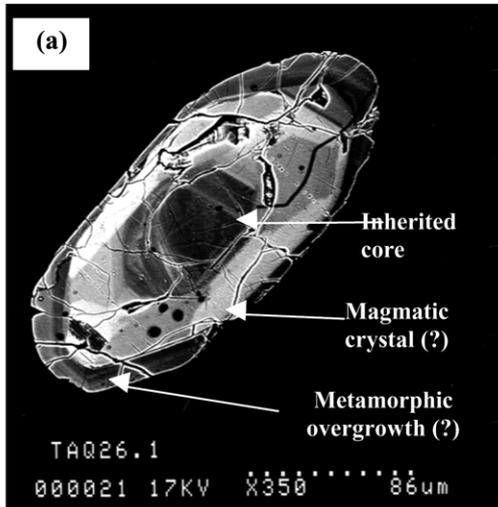


Table 1

Analytical U–Pb data for zircon from monzodioritic orthogneiss. Obs.: All fractions are non-magnetic at 3.0 A power and 2° side tilt on Frantz separator. Sample TAQ 26.1. Geographic coordinates: 07°54′07″S. 36°00′11″W. Symbols: NAb: not abraded; Ab: abraded

| Fraction       | Weight (mg) | U (ppm) | Pb* (ppm) | <sup>206</sup> Pb/ <sup>204</sup> Pb | <sup>207</sup> Pb/ <sup>235</sup> U (error %) | <sup>206</sup> Pb/ <sup>238</sup> U (error %) | <sup>207</sup> Pb/ <sup>206</sup> Pb (error %) | <sup>207</sup> Pb/ <sup>206</sup> Pb (age Ma) |
|----------------|-------------|---------|-----------|--------------------------------------|---|---|--|---|
| A (50–100 μm)  | 0.31 (NAb)  | 201.1   | 58.4      | 5517                                 | 4.32811 (±0.18)                               | 0.25974 (0.11)                                | 0.12085 (0.07)                                 | 1969 ± 3 Ma                                   |
| B (50–100 μm)  | 0.32 (Ab)   | 193.4   | 55.2      | 3840                                 | 4.23942 (0.18)                                | 0.25397 (0.11)                                | 0.12106 (0.07)                                 | 1972 ± 13 Ma                                  |
| C (100–250 μm) | 0.48 (Ab)   | 156.8   | 48.5      | 5963                                 | 4.53578 (0.19)                                | 0.27296 (0.13)                                | 0.12052 (0.06)                                 | 1964 ± 2 Ma                                   |
| D (100–250 μm) | 0.58 (Ab)   | 177.2   | 60.9      | 4943                                 | 5.18937 (0.16)                                | 0.31063 (0.11)                                | 0.12116 (0.05)                                 | 1975 ± 5 Ma                                   |

measured using, respectively, a MAT-262 mass spectrometer and a VG354 at São Paulo University. <sup>87</sup>Sr/<sup>86</sup>Sr data were normalized to <sup>86</sup>Sr/<sup>88</sup>Sr = 0.1194, and the age was calculated according to Ludwig (1999) with  $\lambda_{Rb} = 1.42 \times 10^{-11} \text{ yr}^{-1}$ . Nd data were normalized to <sup>146</sup>Nd/<sup>144</sup>Nd = 0.7219 and regression calculations were done with the following constants:  $\lambda_{Sm} = 6.54 \times 10^{-12} \text{ yr}^{-1}$ , actual <sup>143</sup>Nd/<sup>144</sup>Nd<sub>CHUR</sub> = 0.512638 and <sup>147</sup>Sm/<sup>144</sup>Nd<sub>CHUR</sub> = 0.1967. Depleted mantle (DM) values of DePaolo (1981) were used for model ages calculation. Errors on isotopic ratios and ages are given at 2σ level.

#### 4.1. U–Pb dating of quartz monzodioritic orthogneisses

Four zircon fractions were analyzed for U–Pb (Table 1). A further fraction (E) of prismatic bipyramidal coarse and brown zircons was not analyzed because the crystals are fractured and show complex internal structures (Fig. 5(a) and (b)).

Fraction A is composed of small light and transparent elongate bipyramidal-prismatic and thin crystals (length/width ratio  $l/w \approx 4$ ). SEM images (back-scattered electron mode) of pale-yellow crystals show tiny inclusions and suggest inherited cores and metamorphic or magmatic overgrowth rims (Fig. 5(c)). Such complex crystals were avoided in the analyzed fractions. These thin needle-shaped crystals were not submitted to abrasion. Fraction B also presents bipyramidal and prismatic crystals similar to those of fraction A, but crystals are wider ( $l/w \approx 2.5$ ) and all of them are yellowish in color. The analyzed grains do not present inclusions, inherited cores or overgrowths. Fraction C is composed of larger crystals (100–250 μm), and also bipyramidal prismatic ( $l/w \approx 2.5$ ), colorless to pale yellow; no core was observed on SEM images, but they

show metamict rims. Fraction D is composed of short-prismatic crystals ( $l/w \approx 1.0$ – $1.5$ ), all being colorless.

The four analyzed zircon fractions from the quartz monzodioritic orthogneiss are discordant and poorly aligned (MSWD = 76). The corresponding upper intercept is at  $1974 \pm 32 \text{ Ma}$  (Fig. 6). The weighted average of the <sup>207</sup>Pb/<sup>206</sup>Pb ages is  $1967 \pm 30 \text{ Ma}$  (95% confidence level and 0.99 probability of fit). As the analyzed crystals are always light and transparent, with an idiomorphic bipyramidal–prismatic shape and apparently no overgrowth metamorphic rim, the zircons represent primary igneous minerals and the result is interpreted as the crystallization age of the quartz monzodioritic orthogneiss, which represents a minimum age for the basement rocks.

#### 4.2. U–Pb dating of augen gneisses

The augen gneisses are coarse-grained rocks with large microcline megacrysts up to several centimeters in length in the most deformed domains. The mineral assemblage comprises microcline (>45%), quartz (15–30%), plagioclase (Na-oligoclase, 5–25%) and biotite + amphibole (5–20%), and accessory minerals such as apatite, allanite (sometimes with epidote substitution in crystal borders), garnet, magnetite, fluorite, sphene, and zircon. From modal analyses, the augen gneisses are in the syenogranite to monzogranite fields, according to Streckeisen's (1976) classification. In the field, the rocks show some compositional differences, with predominating amphibole (hastingsite) or biotite. Near Taquaritinga, the subhorizontal foliation (S<sub>2</sub>) exhibits a migmatitic texture with the occurrence of veins of anatectic melts and neof ormation of microcline and interstitial garnet + amphibole + opaque minerals.

Fig. 5. Photos from the SEM obtained on zircons from quartz monzodioritic orthogneiss and augen gneiss of the Taquaritinga region, before final hand picking and abrasion: (a) fractured zircon possibly with three development stages displaying a possible inherited core surrounded by a magmatic crystal (lighter) in turn surrounded by a darker (poorer in U?) overgrowth metamorphic rim. Fraction E, quartz monzodioritic orthogneiss, not chemically analyzed; (b) zircon exhibiting a nebulitic complex structure suggesting one or more (heritage?) nuclei with a possible secondary crystallization. Fraction E, monzodioritic quartz orthogneiss, not chemically analyzed; (c) prismatic elongate crystal exhibiting thin white and dark bands representing magmatic growth zoning, with a possible metamorphic overgrowth on the borders. Fraction A, monzodioritic quartz orthogneiss; (d) homogeneous zircon with some inclusions and no evidence of inherited nucleus or growth and overgrowth textures. The white thin homogeneous contour is a border effect in the SEM. Fraction C of the augen gneiss; (e) Basal section of a zircon crystal with nebulitic center and a primary growth zoning, displaying a metamorphic overgrowth well seen in the right and left borders. Fraction C of the augen gneiss. Crystals from Fig. 5(a) and (b) have not been used for dating since they have complex textures and their results should not represent a single geologic event.

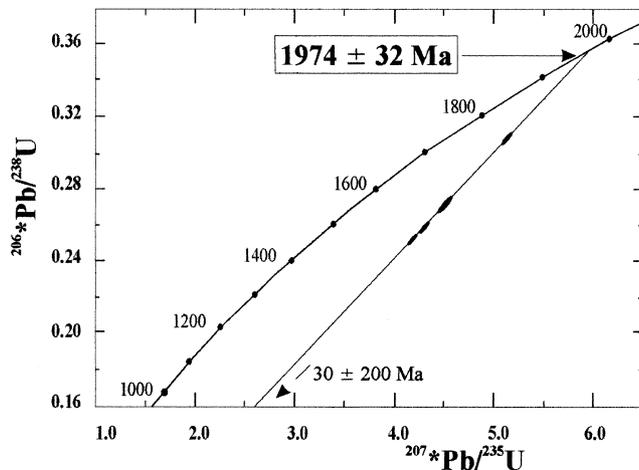


Fig. 6. U–Pb discordia diagram of zircon fractions from quartz monzodioritic orthogneiss of the basement. See Table 1 for details.

Five zircon fractions were analyzed (Table 2). This rock has a significant amount of well-developed, euhedral to subhedral zircons.

The largest crystals were selected in Fraction A, which present elongated shapes up to 300  $\mu\text{m}$  long and 100  $\mu\text{m}$  wide. They are prismatic with a square base, always light, colorless and transparent. SEM images show a growth zoning of magmatic origin and common rounded quartz inclusions. Some crystals exhibit a very thin and continuous light rim, interpreted as a metamorphic (or late magmatic) overgrowth.

Fraction B is composed of well-developed bipyramidal zircons but with short-prismatic shape ( $l/w \approx 1.5$ ); magmatic growth zoning was rarely seen on SEM. These crystals are texturally homogeneous. As they do not show metamict borders or metamorphic overgrowth, they were not abraded.

Crystals of Fraction C are thinner and longer ( $l/w > 3$ ) than those of fraction B. They present a prismatic-rectangular shape and are colorless and transparent. Some crystals are homogeneous on SEM images (Fig. 5(d)), but others present a clear growth zoning (magmatic) indicated by ‘compositional’ alternation (Fig. 5(e)) and inclusions of quartz, apatite, albite, K-feldspar, and monazite. This last mineral is the most abundant inclusion despite the fact that it does not exist as free crystals in the rock; the monazite

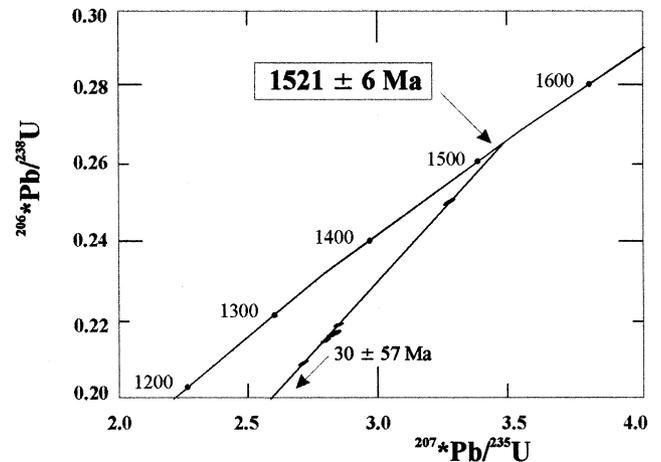


Fig. 7. U–Pb discordia diagram of zircon fractions from augen gneiss. See Table 2 for details.

inclusions have always ellipsoidal shapes and are parallel to growth zoning. Indicative textures of inherited cores have not been detected in this fraction.

Short-prismatic ( $l/w \approx 1$ ), limpid, colorless, and transparent crystals compose fraction D. They do not show inclusions, and some specimens exhibit growth zoning and/or a thin and lighter rim that may indicate metamorphic overgrowth. They are usually homogeneous on SEM images, with some small and round-shaped quartz inclusions. As zircon grains are very small and as overgrowth is rare, they were not abraded.

The five zircon fractions of the augen gneiss sample define a well-aligned discordia (MSWD = 1.8) with an upper intercept age of 1521  $\pm$  6 Ma, shown in Fig. 7. Using the same reasoning as for the orthogneisses, this result represents the crystallization age of the Taquaritinga augen gneiss, but the obtained age is better defined. A significant time gap exists thus between this unit and the basement it intrudes.

#### 4.3. Rb–Sr dating of augen gneisses

Whole-rock Rb–Sr analyses have been performed on six samples of the Taquaritinga augen gneiss. Analytical data are displayed in Table 3, and yield an age of 1376  $\pm$  130

Table 2

Analytical U–Pb data for zircon from augen gneiss. Obs: All fractions are non-magnetic at 3.0 A power and 0° side tilt on Frantz separator. Sample TAQ 26. Geographic coordinates: 07°54'18"S. 36°00'21"W. Symbols: NAb: not abraded. Ab: abraded

| Fraction                   | Weight (mg) | U (ppm) | Pb* (ppm) | $^{206}\text{Pb}/^{204}\text{Pb}$ | $^{207}\text{Pb}/^{235}\text{U}$ (error %) | $^{206}\text{Pb}/^{238}\text{U}$ (error %) | $^{207}\text{Pb}/^{206}\text{Pb}$ (error %) | $^{207}\text{Pb}/^{206}\text{Pb}$ (age Ma) |
|----------------------------|-------------|---------|-----------|-----------------------------------|--|--|---|--|
| A (100–250 $\mu\text{m}$ ) | 0.69 (Ab)   | 113.2   | 33.0      | 2252                              | 3.30408 (0.20)                             | 0.25313 (0.09)                             | 0.09467 (0.11)                              | 1521 $\pm$ 5 Ma                            |
| B (100–250 $\mu\text{m}$ ) | 0.59 (NAb)  | 148.1   | 36.4      | 2492                              | 2.83694 (0.23)                             | 0.21674 (0.13)                             | 0.09493 (0.10)                              | 1527 $\pm$ 4 Ma                            |
| C (100–250 $\mu\text{m}$ ) | 0.99 (Ab)   | 141.0   | 35.9      | 605                               | 2.86744 (0.75)                             | 0.21863 (0.18)                             | 0.09512 (0.61)                              | 1530 $\pm$ 9 Ma                            |
| D (50–100 $\mu\text{m}$ )  | 0.15 (Ab)   | 157.1   | 48.7      | 662                               | 2.81964 (0.39)                             | 0.21537 (0.12)                             | 0.09495 (0.29)                              | 1528 $\pm$ 6 Ma                            |
| E (50–100 $\mu\text{m}$ )  | 0.99 (NAb)  | 154.3   | 37.4      | 2153                              | 2.73345 (0.24)                             | 0.20906 (0.14)                             | 0.09483 (0.10)                              | 1525 $\pm$ 3 Ma                            |

Table 3  
Analytical data for Rb–Sr whole rock samples of augen gneisses

| Samples | Rb (ppm) | Sr (ppm) | $^{87}\text{Rb}/^{86}\text{Sr}$ | $^{87}\text{Sr}/^{86}\text{Sr}(1\sigma)$ | Geographic coordinates |
|---------|----------|----------|---------------------------------|--|------------------------|
| TAQ8A   | 134      | 213      | 1.8270 ( $\pm 0.0360$ )         | 0.74646 ( $\pm 0.00004$ )                | 07°57'57"S, 36°07'27"W |
| TAQ8B   | 139      | 208      | 1.9410 ( $\pm 0.0380$ )         | 0.74884 ( $\pm 0.00003$ )                |                        |
| TAQ26A  | 219      | 130      | 4.9220 ( $\pm 0.0960$ )         | 0.80809 ( $\pm 0.00004$ )                | 07°54'18"S, 36°00'21"W |
| TAQ26B  | 168      | 176      | 2.7780 ( $\pm 0.0550$ )         | 0.76511 ( $\pm 0.00003$ )                |                        |
| TAQ14D  | 118      | 279      | 1.2270 ( $\pm 0.0240$ )         | 0.73644 ( $\pm 0.00003$ )                | 07°53'59"S, 36°03'13"W |
| TAQ14E  | 128      | 224      | 1.6590 ( $\pm 0.0330$ )         | 0.74070 ( $\pm 0.00003$ )                |                        |

Ma (MSWD = 6.9) and a  $^{87}\text{Sr}/^{86}\text{Sr}$  initial ratio of  $0.7104 \pm 0.0045$  (Fig. 8). The points on the diagram are not well aligned. They include two samples (14D and 14E) from migmatized augen gneisses with metamorphic amphibole + microcline + garnet. If we exclude these two migmatized samples, the calculated age is  $1380 \pm 43$  Ma ( $R_0 = 0.7102$  and MSWD = 0.04), which is probably a better age estimate. However, the  $>100$  Ma age difference with respect to the U–Pb age of the same magmatic unit and the worst alignment of the migmatized samples suggest that the Rb–Sr isotopic system may have been somewhat affected by  $F_2$  and  $F_3$  tectonometamorphic events. This fact deviates from the results of chemical analysis that suggest (see below) that at least for the whole-rock the chemical system remained closed during metamorphism. Such a difference between Rb–Sr and U–Pb ages cannot be explained only by different closure temperatures.

#### 4.4. Sm–Nd model age of augen gneisses

Sm–Nd analyses were performed on two samples of the Taquaritinga augen gneiss unit (Table 4), which yielded  $\varepsilon_{\text{Nd}(1.52)}$  values of  $-10.45$  and  $-8.79$  and  $T_{\text{DM}} \approx 2.5$  Ga, as displayed in Fig. 9. These  $\varepsilon_{\text{Nd}}$  values, in addition to a relatively high  $^{87}\text{Sr}/^{86}\text{Sr}$  initial ratio of  $0.71128$ , strongly suggest a crustal component in the augen gneiss protolith.

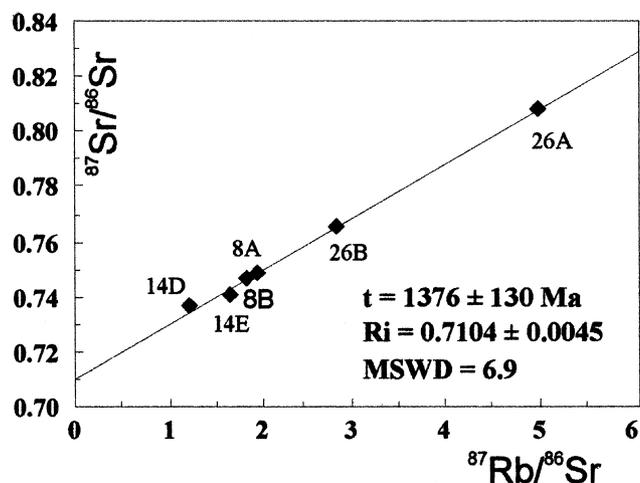


Fig. 8. Rb–Sr whole-rock isochron for augen gneiss. Data in Table 3.

## 5. Geochemistry

### 5.1. Taquaritinga augen gneisses

Chemical analyses of major, minor, and trace elements (including REE) were performed for the augen gneisses (Table 5). Samples numbered 14 are from the earlier-mentioned migmatite sites. On these samples tests were done to verify elements' mobility produced by migmatization using Grant's method (Grant, 1986) together with other tools like Harker's diagrams, to compare samples with and without garnet. It was shown that there was no obvious element mobility due to metamorphism from a comparison of these samples. On this basis, chemical results may be used to establish the geochemical affinities of the augen gneisses and their geodynamic signatures.

Chemically, the Taquaritinga augen gneiss is a homogeneous and evolved unit with  $\text{SiO}_2$  content varying from 68.5 to 73%. They are high in alkaline elements ( $\text{Na}_2\text{O} + \text{K}_2\text{O} \approx 8\%$ ) with prominent K and Fe, and relatively low Al ( $\text{Al}_2\text{O}_3 < 14\%$ ) and Mg contents. They present a metaluminous character attested by the negative values of the A-parameter ( $\text{Al} - (\text{Na} + \text{K} + 2\text{Ca}) < 0$ ) of Debon and LeFort (1983) and by the Shand index (Fig. 10).

The trace element composition presents high Ba, Zr, and Y contents, as well as rare earth elements ( $\Sigma\text{REE}$  from 300 to 1500 ppm). The chondrite-normalized REE diagrams (Fig. 11(a)) are characterized by a high fractionation for LREE ( $\text{La}_N/\text{Yb}_N \approx 4.5$ ), a low one for HREE ( $\text{Gd}_N/\text{Yb}_N \approx 1.9$ ), and a strong negative Eu anomaly ( $\text{Eu}_N/\text{Eu}_N \leq 0.5$ ). All these chemical characteristics, together with a relatively large amount of fluorite, apatite, and magnetite, are generally observed in A-type granites (Loiselle and Wones, 1979). A similar A-type affinity is also shown in the  $(\text{K}_2\text{O} + \text{Na}_2\text{O})/\text{CaO}$  vs  $\text{Zr} + \text{Nb} + \text{Ce} + \text{Y}$  diagram (Fig. 12).

Using the tectonic discrimination diagrams, the ca. 1.5 Ga augen gneisses plot in the within-plate field (Fig. 13), a tectonic signature also attested by multi-elemental spidergrams (Fig. 14), which exhibit patterns similar to that presented by the within-plate Sabaloka granite (Pearce et al., 1984) and by anorogenic granites described by Roger and Greenberg (1990). We therefore conclude that the Taquaritinga augen gneiss is an A-type granite and

Table 4

Analytical data for Sm–Nd whole rock samples of augen gneisses.  $T_{DM}$  model ages following model of DePaolo (1981)

| Samples | Sm (ppm) | Nd (ppm) | $^{147}\text{Sm}/^{144}\text{Nd}$ | $^{143}\text{Nd}/^{144}\text{Nd}$ | $\epsilon_{\text{Nd}}(1.52 \text{ Ga})$ | $T_{DM}$ | Geographic coordinates |
|---------|----------|----------|-----------------------------------|-----------------------------------|---|----------|------------------------|
| TAQ8B   | 22.82    | 136      | 0.095418 ( $\pm 0.000050$ )       | 0.511102 ( $\pm 0.000038$ )       | – 10.45                                 | 2.52     | 07°57'57"S, 36°07'27"W |
| TAQ26A  | 30.89    | 155      | 0.110244 ( $\pm 0.000056$ )       | 0.511335 ( $\pm 0.000036$ )       | – 8.79                                  | 2.53     | 07°54'18"S, 36°00'21"W |

represents a relatively homogeneous and evolved meta-luminous igneous suite, with no intermediate terms, generated and emplaced in an anorogenic setting.

### 5.2. Basement orthogneisses

Chemical analyses of basement granodioritic orthogneisses, which were intruded by the 1.97 Ga quartz monzodioritic orthogneisses, were also carried out for six samples from the northwestern part of the studied area. They are mesocratic and texturally homogeneous rocks, with some millimetric garnet and feldspar crystals. These rocks exhibit a tectonic foliation and a thin and continuous banding interpreted as the result of metamorphic differentiation. The mineral assemblage comprises plagioclase (Ca-oligoclase, 25–35%), quartz (30–35%), microcline (10–20%), biotite (5–15%), hornblende (1–8%), and garnet (1–5%), with sphene, opaque minerals, epidote, apatite, and zircon as accessory minerals.

Chemical data (Table 5) indicate that the basement orthogneisses have a high alkaline content with a dominantly sodic character and that they are richer in Ca, Al, and Sr than the augen gneisses. Rb, Y, Zr, and rare earth elements contents show low values (mainly LREE). The REEs present a highly fractionated (Fig. 10(b)) pattern ( $L_{a_N}/Y_{b_N} \approx 15$ ) with a small but positive Eu anomaly, which may be due to their high plagioclase content. In the alumina index diagram (Fig. 10) these samples plot in the transition between the metaluminous and peraluminous fields.

The geochemical features of the basement granodioritic

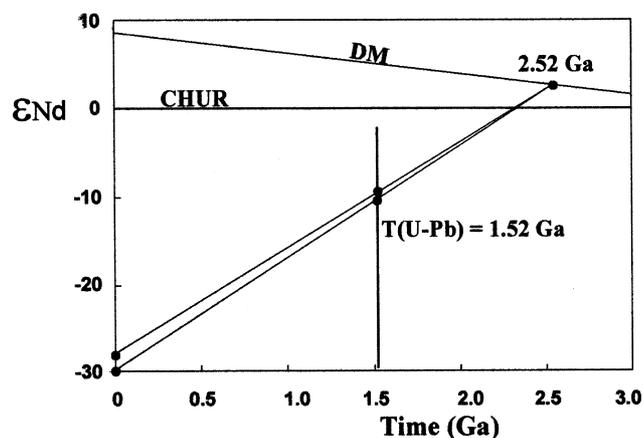


Fig. 9.  $^{143}\text{Nd}/^{144}\text{Nd}$  evolution (represented by  $\epsilon_{\text{Nd}}$ ) vs time, for the augen gneiss. Points in the central part represent  $\epsilon_{\text{Nd}}$  values at the time of crystallization. DM values from DePaolo (1981).

orthogneisses of Taquaritinga region are similar to that presented by calcalkaline granites and, according to Pearce diagram (Fig. 13), they have a chemical signature similar to volcanic arc granites (VAG). All these data suggest that they correspond to calcalkaline granites generated in a volcanic arc geodynamic setting.

## 6. Discussion

### 6.1. Age of the basement

Field observations show that the Taquaritinga augen gneisses cross-cut the  $S_1$  metamorphic banding of the basement rocks. This implies that the banding was formed before 1.52 Ga. As a monzodioritic orthogneiss from the basement is dated at 1.97 Ga and cross-cuts also the banding of the surrounding gneisses, the basement protoliths are attributed to an early Proterozoic event. However, the dated monzodioritic orthogneiss shows the same  $S_1$  and  $L_x^1$  tectonic fabric that occurs in the banded gneisses, this fabric being in turn cross-cut by the Taquaritinga augen gneiss. Consequently, the 1.97 Ga orthogneiss corresponds probably to a syn- to late-tectonic Transamazonian intrusive and the granodioritic orthogneisses and banded gneisses would represent earlier stages of this Transamazonian orogeny (Figs. 2 and 4). In this sense, we remark that the geochemical features of these granodioritic orthogneisses suggest that they represent a syntectonic crustal accretion, in such a case linked to the Paleoproterozoic Transamazonian/Eburnean orogenic event.

Several lines of evidence support this assumption: (1) a zircon fraction from the monzodioritic orthogneiss was described earlier, though not analyzed (fraction E, Fig. 5(a) and (b)) because the corresponding zircons exhibit complex development stages, including inherited cores; (2) in the Caldas Brandão region, about 100 km northeast of Taquaritinga, Fernandes and Brito Neves (1998) obtained U–Pb ages of ca. 2.2 Ga for older basement orthogneiss ( $\text{Nd } T_{DM} = 2.34\text{--}2.72 \text{ Ga}$ ), attesting to the Paleoproterozoic age, at least pro-part, for orthogneisses and banded gneisses very similar to those of the Taquaritinga region; (3) in the Alto Pajeú Terrain, another region of the TZ, an age of  $2052 \pm 13 \text{ Ma}$  was recently determined on a migmatitic basement gneiss (Paul Leite, verbal comm.).

The chemical data from the granodioritic orthogneisses occurring in the Taquaritinga basement show calcalkaline character with geochemical signature similar to that presented by VAG. This suggests that this basement unit

Table 5  
Chemical analysis from Paleo and Mesoproterozoic plutonic rocks

|                                | Augen gneisses |       |       |       |       |       |       |       |       |       |       |       |       |       | Granodioritic orthogneisses (basement) |       |       |  |  |  |  |  |  |  |  |  |  |  |
|--------------------------------|----------------|-------|-------|-------|-------|-------|-------|-------|-------|-------|-------|-------|-------|-------|--|-------|-------|--|--|--|--|--|--|--|--|--|--|--|
|                                | 8A             | 8B    | 9     | 19    | 26A   | 26B   | 26C   | 14A   | 14C   | 14D   | 14E   | 1A    | 1B    | 1C    | 1D                                     | 1E    | 1F    |  |  |  |  |  |  |  |  |  |  |  |
| SiO <sub>2</sub>               | 69.78          | 69.84 | 70.81 | 72.76 | 70.95 | 69.93 | 70.72 | 69.23 | 70.84 | 68.71 | 69.62 | 69.69 | 70.00 | 69.19 | 70.00                                  | 69.94 | 68.01 |  |  |  |  |  |  |  |  |  |  |  |
| TiO <sub>2</sub>               | 0.48           | 0.39  | 0.29  | 0.28  | 0.37  | 0.41  | 0.38  | 0.43  | 0.42  | 0.42  | 0.46  | 0.25  | 0.25  | 0.26  | 0.25                                   | 0.25  | 0.28  |  |  |  |  |  |  |  |  |  |  |  |
| Al <sub>2</sub> O <sub>3</sub> | 13.47          | 13.27 | 13.08 | 11.85 | 12.76 | 13.25 | 13.11 | 13.53 | 12.63 | 13.52 | 13.13 | 15.25 | 15.22 | 15.35 | 15.29                                  | 15.38 | 15.72 |  |  |  |  |  |  |  |  |  |  |  |
| Fe <sub>2</sub> O <sub>3</sub> | 5.25           | 4.54  | 3.80  | 4.14  | 5.00  | 4.82  | 4.41  | 4.97  | 5.16  | 4.95  | 4.92  | 2.86  | 2.78  | 2.96  | 2.65                                   | 2.84  | 2.91  |  |  |  |  |  |  |  |  |  |  |  |
| MnO                            | 0.06           | 0.05  | 0.04  | 0.04  | 0.05  | 0.05  | 0.04  | 0.05  | 0.07  | 0.04  | 0.06  | 0.05  | 0.05  | 0.05  | 0.02                                   | 0.05  | 0.05  |  |  |  |  |  |  |  |  |  |  |  |
| MgO                            | 0.29           | 0.19  | 0.09  | 0.03  | 0.11  | 0.16  | 0.13  | 0.16  | 0.13  | 0.22  | 0.15  | 0.55  | 0.64  | 0.63  | 0.47                                   | 0.57  | 0.65  |  |  |  |  |  |  |  |  |  |  |  |
| CaO                            | 1.79           | 1.69  | 1.44  | 1.57  | 1.83  | 1.82  | 1.70  | 1.82  | 1.92  | 2.00  | 1.96  | 2.32  | 2.69  | 2.52  | 2.29                                   | 2.55  | 2.37  |  |  |  |  |  |  |  |  |  |  |  |
| Na <sub>2</sub> O              | 3.25           | 3.17  | 2.96  | 2.51  | 2.89  | 3.02  | 2.98  | 3.13  | 3.04  | 3.23  | 3.06  | 4.13  | 4.39  | 4.47  | 3.73                                   | 4.46  | 4.20  |  |  |  |  |  |  |  |  |  |  |  |
| K <sub>2</sub> O               | 4.70           | 5.18  | 5.66  | 5.38  | 5.36  | 5.42  | 5.49  | 5.44  | 4.72  | 5.48  | 5.15  | 3.66  | 2.94  | 3.18  | 4.32                                   | 3.03  | 3.88  |  |  |  |  |  |  |  |  |  |  |  |
| P <sub>2</sub> O <sub>5</sub>  | 0.11           | 0.08  | 0.07  | 0.03  | 0.08  | 0.08  | 0.06  | 0.09  | 0.08  | 0.08  | 0.10  | 0.09  | 0.10  | 0.10  | 0.08                                   | 0.10  | 0.14  |  |  |  |  |  |  |  |  |  |  |  |
| PF                             | 0.77           | 0.82  | 0.92  | 0.93  | 0.56  | 0.66  | 0.56  | 0.56  | 0.59  | 0.66  | 0.56  | 0.63  | 0.73  | 0.92  | 0.46                                   | 0.69  | 0.92  |  |  |  |  |  |  |  |  |  |  |  |
| Total                          | 99.95          | 99.22 | 99.16 | 99.52 | 99.96 | 99.62 | 99.58 | 99.41 | 99.6  | 99.31 | 99.17 | 99.48 | 99.79 | 99.63 | 99.56                                  | 99.87 | 99.13 |  |  |  |  |  |  |  |  |  |  |  |
| Ba                             | 1944           | 1860  | 1471  | 1288  | 1220  | 1648  | 1856  | 2055  | 1835  | 2232  | 2011  | 1253  | 1017  | 1218  | 1497                                   | 981   | 3478  |  |  |  |  |  |  |  |  |  |  |  |
| Cr                             | 186            | 213   | 229   | 190   | 174   | 199   | 214   | 197   | 209   | 188   | 170   | 200   | 199   | 162   | 193                                    | 215   | 212   |  |  |  |  |  |  |  |  |  |  |  |
| Cu                             | 6.8            | 9.1   | 6.4   | 10.6  | 7.8   | 8.5   | 8.1   | 19.00 | 11.8  | 15.7  | 9.2   | 15.3  | 11.3  | 14.8  | 20.0                                   | 9.1   | 11.1  |  |  |  |  |  |  |  |  |  |  |  |
| Ga                             | 25.7           | 26.0  | 29.4  | 29.7  | 32.3  | 26.1  | 25.2  | 28.2  | 24.7  | 26.7  | 25.7  | 19.7  | 18.1  | 19.5  | 18.2                                   | 19.4  | 20.8  |  |  |  |  |  |  |  |  |  |  |  |
| Nb                             | 41.6           | 31.4  | 44.6  | 61.7  | 61.2  | 38.7  | 36.8  | 36.1  | 36.9  | 38.8  | 36.6  | 4.4   | 3.9   | 6.2   | 4.1                                    | 5.4   | 11.5  |  |  |  |  |  |  |  |  |  |  |  |
| Ni                             | 4.4            | 4.2   | 4.4   | 3.8   | 3.8   | 3.8   | 4.4   | 4.6   | 4.3   | 6.5   | 3.8   | 5.3   | 8.7   | 4.4   | 5.1                                    | 5.4   | 6.2   |  |  |  |  |  |  |  |  |  |  |  |
| Rb                             | 134            | 139   | 234   | 177   | 219   | 168   | 154   | 132   | 110   | 118   | 128   | 97.6  | 84.8  | 85.5  | 103                                    | 90.6  | 97.7  |  |  |  |  |  |  |  |  |  |  |  |
| Sr                             | 213            | 208   | 136   | 112   | 130   | 176   | 196   | 234   | 205   | 279   | 224   | 452   | 430   | 494   | 504                                    | 464   | 1101  |  |  |  |  |  |  |  |  |  |  |  |
| Sc                             | 5.3            | 4.7   | 4.2   | 4.1   | 5.4   | 5.0   | 4.4   | 5.6   | 5.3   | 5.9   | 5.1   | 3.7   | 4.3   | 4.1   | 3.7                                    | 4.1   | 4.5   |  |  |  |  |  |  |  |  |  |  |  |
| Th                             | 23.8           | 30.2  | 20.6  | 44.3  | 33.9  | 24.1  | 31.0  | 52.8  | 32.3  | 17.8  | 16.8  | 7.9   | 6.0   | 1.8   | 32.1                                   | 7.9   | 13.8  |  |  |  |  |  |  |  |  |  |  |  |
| V                              | 19.3           | 17.8  | 19.1  | 16.1  | 13.8  | 16.5  | 18.7  | 18.4  | 20.1  | 20.0  | 16.6  | 24.7  | 27.1  | 22.2  | 23.3                                   | 27.8  | 28.5  |  |  |  |  |  |  |  |  |  |  |  |
| Y                              | 80.0           | 74.0  | 94.4  | 140.0 | 133.0 | 83.7  | 73.6  | 73.5  | 79.3  | 77.1  | 67.7  | 9.91  | 7.68  | 6.68  | 5.72                                   | 8.43  | 7.84  |  |  |  |  |  |  |  |  |  |  |  |
| Zn                             | 100.0          | 91.5  | 94.4  | 102.0 | 123.0 | 101.0 | 85.0  | 89.2  | 90.1  | 97.0  | 84.8  | 38.4  | 35.2  | 47.3  | 31.7                                   | 44.6  | 51.7  |  |  |  |  |  |  |  |  |  |  |  |
| Zr                             | 721            | 655   | 506   | 660   | 661   | 647   | 600   | 595   | 599   | 568   | 636   | 130   | 112   | 132   | 216                                    | 127   | 192   |  |  |  |  |  |  |  |  |  |  |  |
| La                             | 161            | 186   | 79    | 329   | 201   | 156   | 189   | 377   | 248   | 151   | 150   | 33    | 30    | 22    | 71                                     | 29    | 56    |  |  |  |  |  |  |  |  |  |  |  |
| Ce                             | 315            | 352   | 157   | 616   | 388   | 320   | 354   | 646   | 448   | 316   | 285   | 58    | 52    | 39    | 123                                    | 52    | 104   |  |  |  |  |  |  |  |  |  |  |  |
| Pr                             | 35             | 40    | 18    | 75    | 45    | 39    | 42    | 73    | 52    | 38    | 33    | 6     | 5     | 4     | 12                                     | 6     | 11    |  |  |  |  |  |  |  |  |  |  |  |
| Nd                             | 124            | 136   | 64    | 253   | 155   | 135   | 142   | 223   | 164   | 132   | 113   | 20    | 19    | 16    | 37                                     | 19    | 40    |  |  |  |  |  |  |  |  |  |  |  |
| Sm                             | 24             | 23    | 15    | 49    | 31    | 25    | 25    | 31    | 27    | 25    | 20    | 3     | 3     | 2     | 5                                      | 3     | 6     |  |  |  |  |  |  |  |  |  |  |  |
| Eu                             | 3              | 3     | 3     | 3     | 3     | 3     | 3     | 4     | 4     | 3     | 3     | 1     | 1     | 1     | 1                                      | 1     | 2     |  |  |  |  |  |  |  |  |  |  |  |
| Gd                             | 18             | 18    | 13    | 37    | 26    | 21    | 19    | 25    | 21    | 19    | 16    | 2     | 2     | 2     | 3                                      | 2     | 4     |  |  |  |  |  |  |  |  |  |  |  |
| Tb                             | 3              | 3     | 3     | 6     | 4     | 3     | 3     | 3     | 3     | 3     | 2     | 0     | 0     | 0     | 0                                      | 0     | 0     |  |  |  |  |  |  |  |  |  |  |  |
| Dy                             | 15             | 15    | 17    | 31    | 25    | 17    | 15    | 17    | 17    | 16    | 14    | 2     | 1     | 1     | 1                                      | 2     | 2     |  |  |  |  |  |  |  |  |  |  |  |
| Ho                             | 3              | 3     | 4     | 6     | 5     | 3     | 3     | 3     | 3     | 3     | 3     | 0     | 0     | 0     | 0                                      | 0     | 0     |  |  |  |  |  |  |  |  |  |  |  |
| Er                             | 8              | 7     | 10    | 15    | 15    | 9     | 8     | 8     | 8     | 8     | 7     | 1     | 1     | 1     | 1                                      | 1     | 1     |  |  |  |  |  |  |  |  |  |  |  |
| Tm                             | 1              | 1     | 2     | 2     | 2     | 1     | 1     | 1     | 1     | 1     | 1     | 0     | 0     | 0     | 0                                      | 0     | 0     |  |  |  |  |  |  |  |  |  |  |  |
| Yb                             | 8              | 8     | 10    | 14    | 16    | 9     | 7     | 7     | 8     | 8     | 7     | 1     | 1     | 1     | 1                                      | 1     | 1     |  |  |  |  |  |  |  |  |  |  |  |
| Lu                             | 1              | 1     | 2     | 2     | 2     | 1     | 1     | 1     | 1     | 1     | 1     | 0     | 0     | 0     | 0                                      | 0     | 0     |  |  |  |  |  |  |  |  |  |  |  |
| Total                          | 719            | 796   | 396   | 1437  | 918   | 741   | 812   | 1419  | 1007  | 725   | 656   | 128   | 115   | 89    | 256                                    | 117   | 227   |  |  |  |  |  |  |  |  |  |  |  |

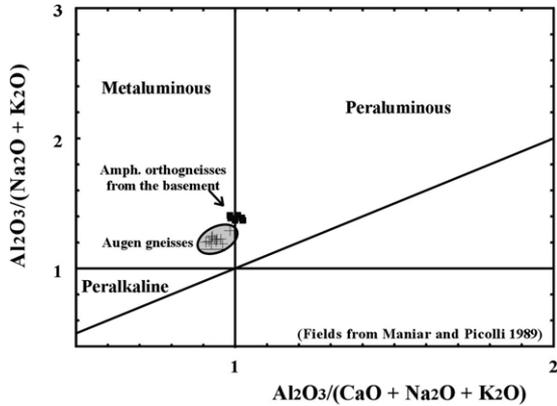


Fig. 10. Diagram using Shand's index for augen gneisses and amphibole orthogneisses. (Fields from Maniar and Picolli, 1989).

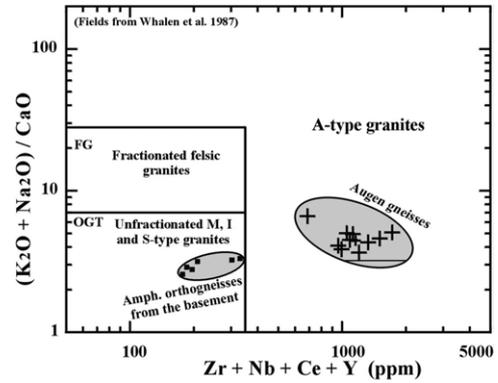


Fig. 12. Zr + Nb + Ce + Y vs  $(K_2O + Na_2O)/CaO$  diagram for augen gneisses and amphibole orthogneisses. (Fields from Whalen et al., 1987).

may have originated during a subduction stage related to the Transamazonian orogeny. The Nd model ages about 2.5 Ga determined for the Taquaritinga augen gneisses indicate the presence of Archean protoliths in this region and are in agreement with  $T_{DM}$  values determined by Fernandes and Brito Neves (1998) for basement rocks of Caldas Brandão, in the north of the Taquaritinga region.

6.2. Significance of the Taquaritinga augen gneisses

Proterozoic igneous activities represented by plutonic and volcanic rocks have been described throughout the

Borborema Province, however, the Taquaritinga augen gneisses represent, so far, the only evidence of igneous emplacement during early Mesoproterozoic (Calimian period, 1.6–1.4 Ga) times. Slightly older (ca. 1.7–1.8 Ga, U–Pb and Rb–Sr) anorogenic augen gneisses and meta-ryolites occur associated with a (meta)sedimentary sequence developed in a rifting process (Jaguaribeian fold belt, Sá et al., 1995), in the northern part of the Borborema Province. Younger events, at the Mesoproterozoic and Neoproterozoic boundary, are also well documented. There are many places where granites and/or metavolcanic rocks were dated in the 1.15–0.95 Ga age range in other

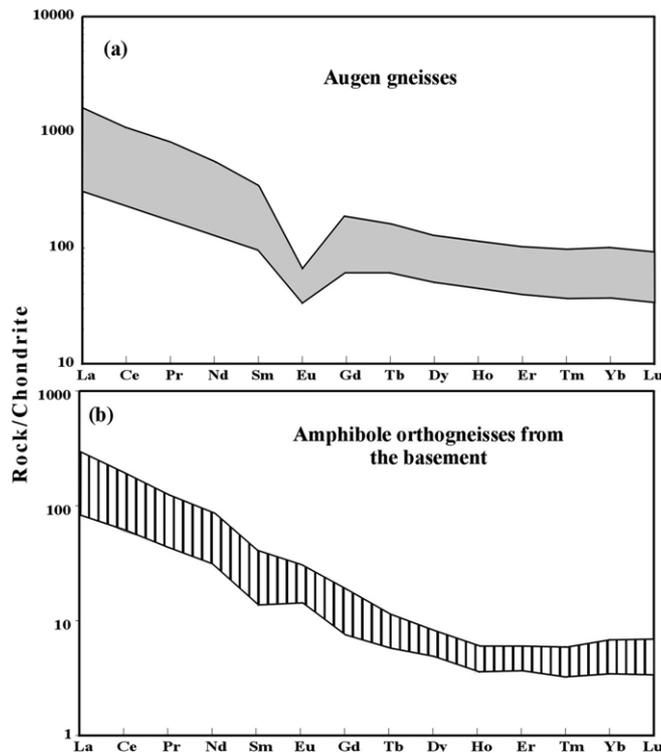


Fig. 11. Chondrite-normalized (Evensen et al., 1978) rare-earth element diagrams for (a) augen gneisses and (b) amphibole orthogneisses. Data in Table 5.

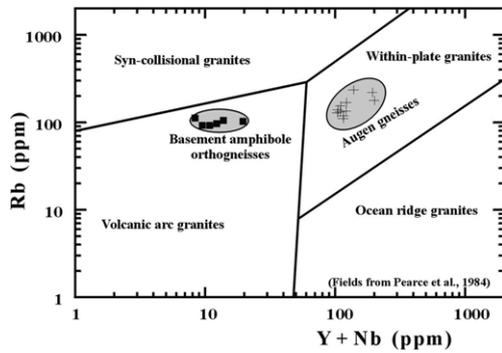


Fig. 13. Tectonic discriminating diagram for Pale- and Mesoproterozoic igneous rocks of Taquaritinga region.

parts of the TZ (Brito Neves et al., 1990; Van Schmus et al., 1995b; Brito Neves et al., 1995a; Santos and Medeiros, 1997; Kozuch et al., 1997). The U–Pb ages at ca. 1.15 Ga presented by Brito Neves et al. (1990) are from a bi-modal metavolcanic association of the Piencó-Alto Brígida fold belt, western part of the TZ.

In the whole Borborema Province and neighboring region, after the Transamazonian orogeny (<1.8 Ga) and up to 1.1 Ga times, there is no record of compressional events or other types of orogenic processes, which indicates that this was a quiescence period in northeastern Brazil in relation to contractional processes (Brito Neves et al., 1995b). All these igneous rocks generated in this time span present anorogenic geochemical signature and frequently are emplaced in sedimentary sequences, implying that the igneous activity was generated and emplaced in a within-plate extensional environment. In this sense, the Taquaritinga augen gneiss, even though it does not present association with volcanic or sedimentary sequences, did witness extensional processes in early Mesoproterozoic times in the eastern part of the TZ of the Borborema Province.

### 6.3. A polycyclic evolution in the TZ?

Available geochronological data in the TZ domain support the existence of (i) a Transamazonian imprint (ca.

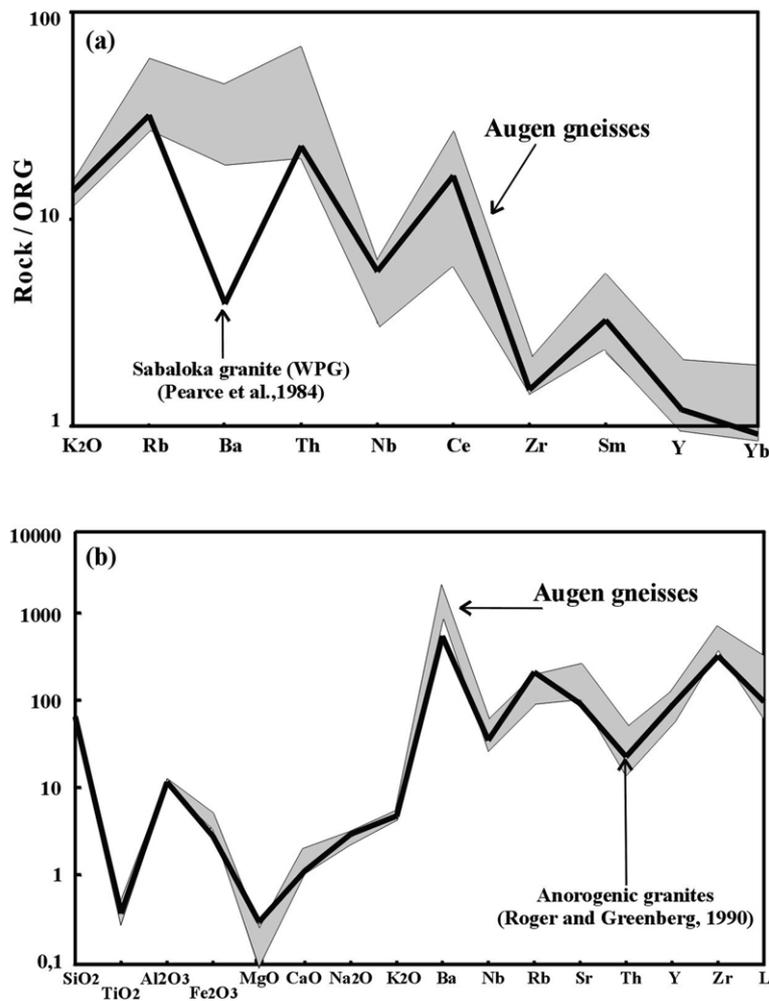


Fig. 14. Discriminant diagrams (spidergrams) of Mesoproterozoic augen gneisses displaying strong chemical similarities with (a) within plate Sabaloka Granite and (b) anorogenic granites of Roger and Greenberg (1990). % weight for oxides and ppm for trace elements were used in (b).

1.95 Ga) restricted to the basement rocks, and (ii) supra-crustal sequences in which tectonic processes occurring by the end of Mesoproterozoic/beginning of Neoproterozoic (ca. 1.0 Ga) era are evidenced.

What did then happen in the Taquaritinga region and what is the tectonic significance of the prominent  $S_2$  sub-horizontal high-grade foliation recorded by the 1.5 Ga Taquaritinga augen gneiss? Two possible interpretations are: (a) these low-angle structures have been formed during the Cariris Velhos orogeny (ca. 1.0 Ga) as suggested from evidence in the central and western part of the TZ, or (b) these structures developed during an early to syntectonic stage of the Brasiliano/Pan-African cycle, before the intrusion of late Neoproterozoic plutons and batholiths.

As already pointed out, the large late Neoproterozoic (ca. 0.6 Ga) plutonic bodies clearly post-date the  $S_2$  sub-horizontal foliation, but, according to Neves and Vauchez (1995) and Neves (1996), the intrusion and emplacement of the Brasiliano granitoids were not controlled by the Fazenda Nova subvertical shear zone, being early to syntectonic with respect to this shear zone.

Considering first hypothesis (b), it is necessary to assume that the Brasiliano processes that eventually formed a low-angle foliation started before the emplacement of the Neoproterozoic intrusives, because all granitoids clearly cross-cut not only the augen gneisses but also its sub-horizontal fabric (see Fig. 4). Consequently, a complete change in tectonic regime must have occurred, separated by a quiescence period, between the subhorizontal tectonic foliation and the primary igneous layering (e.g. PFC-type of Hutton, 1988) described in the Neoproterozoic intrusives (Neves, 1996). Such quiescence would be followed by a second compressive event responsible for the vertical shear zones and mylonites exhibited by the Neoproterozoic plutons and batholiths.

It must be pointed out that there is no clear geochronological information to support the existence of two well-separated stages in the Brasiliano Cycle in this region. The U–Pb and Rb–Sr dating of ca. 592 and 585 Ma, respectively, and Ar–Ar plateau ages of ca. 585 and 555 Ma for amphibole and biotite (Neves, 1996), respectively, rather support a single event registered by different closure temperatures than two compressive Brasiliano pulses verifying the (b) hypothesis.

There is no evidence for a Cariris Velhos age of the subhorizontal  $S_2$  foliation of the Taquaritinga augen gneiss—hypothesis (a). The Rb–Sr result for augen gneisses, although the Rb–Sr whole-rock system is considered as more sensitive to metamorphic processes than zircon U–Pb system, the obtained younger age only suggests some isotopic disturbance which may have occurred either in Cariris Velhos or Brasiliano times. Although the whole-rock system was apparently chemically undisturbed, it was possibly open for Sr isotopes. It was intended to use monazite for U–Pb isotopic analyses, to test the possibility of a younger event but the augen gneisses

do not contain free monazite, except some tiny inclusions in zircons seen on SEM images.

To summarize, there is no conclusive information to verify either (a) or (b) hypothesis. The U–Pb, Rb–Sr, Sm–Nd, and Ar–Ar geochronological methods did not yield indications that the Cariris Velhos orogeny was a crust-forming and/or a major tectonic event in the eastern part of the TZ. Nor do they indicate that the Brasiliano tectonic orogeny comprises two compressional tectonic pulses separated by a quiescence period in which the Neoproterozoic plutons were generated and intruded.

## 7. Concluding remarks

Geochronological data from the eastern part of the TZ, Borborema Province, attest that this region is composed, at least, of Paleoproterozoic (>1.97 Ga), Mesoproterozoic (1.5 Ga), and Neoproterozoic (0.6 Ga) rocks. Nd model ages up to 2.7 Ga for basement rocks (Fernandes and Brito Neves, 1998) and 2.5 Ga for the Taquaritinga augen gneiss also indicate the existence of an Archean crustal component for these igneous suites. In the central and western part of TZ, Van Schmus et al. (1995) and Brito Neves et al. (1995a) recognized a major extensional event that took place during late Mesoproterozoic (1.1 Ga) times. This event was not found by this study in the eastern part of TZ.

The Taquaritinga augen gneiss presents similar textural and structural aspects, with a conspicuous flat-lying foliation, to other common augen gneisses from other parts of the TZ and throughout the Borborema Province. However, the Taquaritinga augen gneiss is alkaline and anorogenic, whereas other units are usually subalkaline to calcalkaline and different in age (e.g. Jardim de Sá, 1994), hence they must not be used as a time reference datum throughout the Borborema Province. Nevertheless, despite being about 500 km apart, it must be outlined that the Taquaritinga augen gneiss shows the same chemical character and geodynamic signatures than the Orós Group augen gneisses (Sá et al., 1995), which are slightly older (ca. 1.7 Ga, U–Pb and Rb–Sr). The occurrence of 1.5 Ga A-type augen gneisses only in the eastern part of the TZ and the lack of evidence for a Cariris Velhos (=Grenville) compressional event in that region may imply that eastern TZ belongs to a distinct geological terrain, as suggested by Santos and Medeiros (1997) who named it Rio Capibaribe Terrain. In such a case, the NE–SW transcurrent Congo shear zone located to the west of the Taquaritinga region could correspond to the structural break that divides the Taquaritinga region (Rio Capibaribe Terrain) from the other geological terrains forming the TZ.

In conclusion, data from several geochronological approaches point out that the Transamazonian event that affected the basement rocks of Taquaritinga region, was

followed by an extensional event at 1.5 Ga and by the Brasiliano/Pan-African orogeny in the late Neoproterozoic.

## Acknowledgements

Grants from CAPES/COFECUB 177/95 Brazil–France Project are gratefully acknowledged. Thanks are due to CRPG/CNRS Laboratory at Nancy, France, for the chemical and U–Pb isotopical analyses as well as K. Sato from Geochronological Research Center of São Paulo University, for measuring Rb–Sr and Sm–Nd on Mass Spectrometer. We wish to thank our colleagues A.C. Galindo, G. Melo Jr., B.B. de Brito Neves and E. Santos for their criticism and helpful discussion. Many thanks are also due to R. Weinberg and M. Babinski for reviewing the manuscript and contributing to the improvement of the paper.

## References

- Almeida, F.F.M., Hasui, Y., Brito Neves, B.B., Fuck, R., 1977. Províncias estruturais brasileiras. Actas do VIII Simpósio de Geologia do Nordeste. Campina Grande, Brazil, pp. 363–391.
- Archânjo, C.J., Bouchez, J.L., 1991. Le Seridó, une chaîne transpressive dextre au Protérozoïque supérieur du Nord-Est du Brésil. Bulletin de la Société Géologique de France 162, 637–647.
- Bertrand, J.M., Jardim de Sá, E.F., 1990. Where are the Eburnian–Transamazonian collisional belts? Canadian Journal Earth Sciences 27, 1382–1393.
- Bertrand, J.M., Guillot, F., Leterrier, J., Perruchiot, M.P., Aillertes, L., Macaudiere, J., 1998. Granitoides de la zone houillère briançonnaise (Alpes occidentales): géologie et géochronologie U–Pb. Geodinamica Acta 11, 33–49.
- Brito Neves, B.B., 1983. O mapa geológico do Nordeste oriental do Brasil, escala 1/1.000.000. Unpublished Livre Docencia Thesis. Instituto de Geociências, Universidade de São Paulo, São Paulo, p. 177.
- Brito Neves, B.B., Van Schmus, W.R., Basei, M.A.S., 1990. Contribuição ao estudo da evolução geocronológica do sistema de dobramentos Piancó–Alto Brígida. Actas XXXVI Congresso Brasileiro de Geologia. Natal, Brazil 6, pp. 2697–2710.
- Brito Neves, B.B., Van Schmus, W.R., Santos, E.J., Campos Neto, M.C., Kozuch, M., 1995a. O evento Cariris Velhos na Província Borborema: integração de dados, implicações e perspectivas. Revista Brasileira de Geociências 25, 279–296.
- Brito Neves, B.B., Sá, J.M., Nilson, A.A., 1995b. A tafrogênese Estateriana nos blocos paleoproterozóicos da América do Sul e processos subsequentes. Geonomos 3, 1–21.
- Caby, R., 1989. Precambrian Terranes of Benin-Nigeria and Northeast Brazil and the Late Proterozoic South Atlantic Fit. Special Paper 230. Geological Society of America pp. 145–158.
- Caby, R., Arthaud, M., 1986. Major precambrian nappes of the Brazilian belt, Ceará, Northeast Brazil. Geology 14, 871–874.
- Debon, F., LeFort, P., 1983. A chemical–mineralogical classification of common plutonic rocks and associations. Transactions Royal Society of Edinburgh: Earth Sciences 73, 135–149.
- DePaolo, D.J., 1981. A neodymium and strontium isotopic study of the Mesozoic calc-alkaline granitic batholiths of the Sierra Nevada and Peninsular Ranges, California. Journal of Geophysical Research 86, 10470–10488.
- Evensen, N.H., Hamilton, P.J., O’Nions, R.K., 1978. Rare earth abundances in chondritic meteorite. Geochimica et Cosmochimica Acta 42, 1199–1212.
- Fernandes, T.M.G., Brito Neves, B.B., 1998. Estratigrafia e geocronologia da parte sul do Maciço Caldas Brandão-PB. Actas XL Congresso Brasileiro de Geologia. Belo Horizonte, Brazil, p. 22.
- Galindo, A.C., Dall’Agnol, R., McReath, I., Lafon, J.M., Teixeira, N., 1995. Evolution of Brasiliano-age granitoid types in a shear-zone environment, Umarizal–Caraúbas region, Rio Grande do Norte, north-east Brazil. Journal of South American Earth Sciences 8, 79–95.
- Grant, J.A., 1986. The Isocon diagram—a simple solution to Gresen’s equation for the metasomatic alteration. Economic Geology 2, 47–65.
- Guimarães, I.P., Silva Filho, A.F., 1997. Nd and Sr isotopes and U–Pb geochronological data constraints for the evolution of the shoshonitic Brasiliano Bom Jardim and Toritama complexes: evidence for vertically layered enriched mantle in northeast Brazil? South America Symposium on Isotope Geology. Campos do Jordão, Brazil, Extended Abstract Volume, pp. 129–130.
- Hutton, D.H.W., 1988. Granite emplacement mechanism and tectonic controls interferences from deformation studies. Transactions Royal Society of Edinburgh: Earth Sciences 79, 245–255.
- Jardim de Sá, E.F., 1994. A Faira Seridó (Província Borborema, NE do Brasil) e o seu significado geodinâmico na Cadeia Brasileira/Pan-Africana. Unpublished PhD Thesis. Universidade de Brasília, Brasília, Brazil, p. 803.
- Jardim de Sá, E.F., 1984. A evolução proterozóica da Província Borborema. Actas XI Simpósio Geologia do Nordeste. Natal, Brazil, pp. 297–316.
- Jardim de Sá, E.F., Hackspacher, P.C., 1980. Reconhecimento estrutural na borda noroeste do Cráton do São Francisco. Actas XXXI Congresso Brasileiro de Geologia. Camboriú, Brazil 5, pp. 2719–2731.
- Kawashita, K., Mantovanni, M., Thomaz Filho, A., Torquato, J.R., Berenholc, M., 1974. Método radiométrico rubídio–estrôncio. Procedimento das análises no Centro de Pesquisas Geocronológicas da Universidade de São Paulo. Manual interno (unpublished report), p. 106.
- Kozuch, M., Van Schmus, W.R., Brito Neves, B.B., 1997. Ages and isotope geochemistry of two pre-Brasiliano magmatic events in the Borborema Province of NE Brazil. South American Symposium on Isotope Geology. São Paulo, Brazil, Extended Abstract Volume, pp. 157–160.
- Loiselle, M.C., Wones, D.R., 1979. Characteristics and origin of anorogenic granites. Geological Society of America, Abs. with Prog. 11, p. 468.
- Ludwig, K.R., 1999. User’s manual for Isoplot/Ex version 2.10. Berkeley Geochronology. Chemical Geology 66, 99–102.
- Macedo, M.H.F., Jardim de Sá, E.F., Sá, J.M., 1984. Datações Rb–Sr em ortognaisses e a idade do Grupo Seridó. Actas XI Simpósio Geologia do Nordeste. Natal, Brazil, pp. 253–262.
- Maniar, P.D., Picolli, P.M., 1989. Tectonic discrimination of granitoids. Geological Society of America Bulletin 101, 635–643.
- McMurry, J., Long, L.E., Sial, A.N., 1987. Petrology and isotope systematics of magma mushes: some porphyritic granitoids of northeastern Brazil. Revista Brasileira de Geociências 17, 473–480.
- Neves, S.P., 1996. Etudes des relations entre magmatisme et zones de cisaillement lithosphériques: exemple des décrochements de Pernambuco e Fazenda Nova—état de Pernambuco—Brésil. Unpublished PhD Thesis. Université de Montpellier, Montpellier, France, p. 243.
- Neves, S.P., Vauchez, A., 1995. Successive mixing and mingling of magmas in a plutonic complex of Northeast Brazil. Lithos 34, 275–299.
- Pearce, J.A., Harris, N.B.W., Andrew, G.T., 1984. Trace element discrimination diagrams for the tectonic interpretation of granitic rocks. Journal of Petrology 25, 956–983.
- Ramsay, J.G., 1967. Folding and fracturing of rocks. McGraw-Hill, New York p. 568.
- Roger, J.J.W., Greenberg, J.K., 1990. Late-orogenic, post-orogenic, and anorogenic granites: distinction by major-element and trace-element chemistry and possible origins. Journal of Geology 98, 291–309.
- Sá, J.M., McReath, I., Leterrier, J., 1995. Petrology, geochemistry and geodynamic setting of Proterozoic igneous suites of the Orós fold belt (Borborema Province, Northeast Brazil). Journal of South American Earth Sciences 8, 299–314.
- Santos, E.J., Medeiros, V., 1997. Constraints from granitic plutonism on Proterozoic crustal growth of the Zona Transversal domain, Borborema

- Province, NE Brazil. Actas II International Symposium on Granites and Associated Mineralization. Salvador, Brazil, Extended Abstract Volume, pp. 237–239.
- Sato, K., Tassinari, C.C.G., Kawashita, K., Petronilho, A., 1995. O método geocronológico Sm–Nd no IG-USP e suas aplicações. *Anais da Academia Brasileira de Ciências* 68, 313–336.
- Souza, L.C., 1996. Zonéographie métamorphique, chimie des minéraux, pétrochimie, géochronologie  $^{40}\text{Ar}/^{39}\text{Ar}$  et histoire P-T-t des mica-schistes englobant le massif gabbro-granitique d'Acari, ceinture mobile du Seridó (NE du Brésil). Unpublished PhD Thesis. Université Catholique de Louvain, Louvain-la-Neuve, Belgium, p. 345.
- Streckeisen, A., 1976. To each plutonic rocks its proper name. *Earth Sciences Review* 12, 1–33.
- Van Schmus, W.R., Brito Neves, B.B., Hackspacher, P., Babinski, M., 1995a. U/Pb and Sm/Nd geochronologic studies of the Eastern Borborema Province, Northeastern Brazil: initial conclusions. *Journal of South American Earth Sciences* 8, 267–288.
- Van Schmus, W.R., Brito Neves, B.B., Hackspacher, P., Babinski, M., Fetter, A., Dantas, E., 1995b. Neoproterozoic and late Mesoproterozoic sedimentary and volcanic sequences in the Borborema Province, NE Brazil. Actas XVI Simpósio Geologia do Nordeste. Recife, Brazil 2, pp. 391–393.
- Whalen, J.B., Kenneth, L.C., Chappel, B.W., 1987. A-type granites: geochemical characteristics, discrimination and petrogenesis. *Contributions to Mineralogy and Petrology* 95, 407–419.